Decentralized Fault-Tolerant Control for Multiple Electric Sail Relative Motion at Artificial Lagrange Points

Wei Wang[(1)], Giovanni Mengali[(2)], Alessandro A. Quarta[(2)], Hexi Baoyin[(1)*]

[(1)] *School of Aerospace Engineering, Tsinghua University, 100084 Beijing, People's Republic of China*

[(2)] *Department of Civil and Industrial Engineering, University of Pisa, I-56122 Pisa, Italy*

Abstract

This paper establishes a distributed fault-tolerant control framework for E-sail relative motion at Sun-Earth artificial Lagrange points, capable of accounting for unexpected E-sail actuator fault like effectiveness loss and bias error. The E-sail relative motion problem is formulated on the linearized dynamics, and the steering control is conducted by suitably adjusting the sail attitude and sail lightness number. The proposed control strategy facilitates the E-sail relative distances to evolve within a bounded range and to synchronously converge to the desired values, while collision avoidance of the relative motion is ensured as well. In particular, the locally shared information among the E-sails is assumed to be characterized by their relative distances only, thus extending the existing results where the inter-sail communication capability is static. The concept of distributing multiple E-sails in cluster flight is useful for the deep-space formation missions such as the DARWIN mission, in which a multi-point measurement of the space environment is required. Illustrative examples show the validity of the proposed method in a typical mission scenario.

Keywords: Electric solar wind sail, Artificial Lagrange points, Distributed control, Collision avoidance

Nomenclature

$\boldsymbol{a}$	=	propulsive acceleration vector [$\mathrm{mm/s^2}$]
$\mathcal{E}$	=	set of edges
$\mathcal{G}$	=	communication topological graph
$\mathbb{H}$	=	healthy indicator matrix
$\mathbb{I}$	=	identity matrix
N	=	number of E-sails
$\boldsymbol{n}$	=	normal vector
$\mathbb{O}$	=	zero matrix
O	=	origin of reference frame
$\boldsymbol{r}$	=	position vector (with $r = \|\boldsymbol{r}\|$), [au]
t	=	time, [days]
$\mathcal{T}$	=	rotating reference frame
$\boldsymbol{u}$	=	control input vector
V	=	potential function
$\mathcal{V}$	=	set of vertices
$\mathbb{W}$	=	weighted adjacency matrix (with entries $[w_{ij}]$)

*Corresponding author

Email addresses: wei_wang@mail.tsinghua.edu.cn (Wei Wang[(1)]), g.mengali@ing.unipi.it (Giovanni Mengali[(2)]), a.quarta@ing.unipi.it (Alessandro A. Quarta[(2)]), baoyin@tsinghua.edu.cn (Hexi Baoyin[(1)])

Published in Aerospace Science and Technology, Vol. 103, August 2020, pp. 105904 (1–12). doi: https://doi.org/10.1016/j.ast.2020.105904

$\hat{\boldsymbol{x}}$, $\hat{\boldsymbol{y}}$, $\hat{\boldsymbol{z}}$	=	unit vectors of rotating reference frame
β	=	sail lightness number
$\boldsymbol{\epsilon}$	=	actuator fault (with $\boldsymbol{\epsilon} \triangleq [\epsilon_\theta,\ \epsilon_\phi,\ \epsilon_\beta]^{\mathrm{T}}$)
θ, ϕ	=	attitude angles, [rad]
μ	=	normalized mass of Earth
$\boldsymbol{\rho}$	=	position vector relative to artificial Lagrange point, [km]
υ	=	vertex of topological graph
$\boldsymbol{\omega}$	=	angular velocity vector (with $\omega = \|\boldsymbol{\omega}\|$), [rad/day]

Subscripts

0	=	artificial Lagrange point
i	=	i-th E-sail
$\oplus$	=	Earth
$\odot$	=	Sun

Superscripts

T	=	transpose
$\cdot$	=	time derivative
$\wedge$	=	unit vector

1. Introduction

In recent years, much effort has been devoted to the study of an Electric Solar Wind Sail (E-sail), which is able to generate a continuous low-thrust by momentum exchange with the incoming ions from the solar wind, without the need of any reaction mass nor any propellant consumption [1]. The peculiarity of such an advanced propulsive concept promotes the feasibility of complex space missions [2, 3, 4, 5, 6], especially when a spacecraft is to be placed for a long time in the nearby of collinear libration points in the Sun-Earth system [7]. In fact, the instability of the resulting orbits requires suitable station keeping maneuvers to be implemented [8, 9].

Recent exemplary missions are the LISA Pathfinder, whose Lissajous orbit around the Lagrangian point L_1 was chosen in order to reach a region with a constant illumination from the Sun and free of gravitational and magnetic disturbances from Earth, and by the Deep Space Climate Observatory (DSCOVR) mission, whose orbit around L_1 closely follows that of Advanced Composition Explorer (ACE) mission in support of real-time solar wind monitoring. By exploiting the essential feature of a propellantless propulsion system, an E-sail may be effectively used to create (and maintain) an artificial point Sunward of L_1 (referred to as AL_1), to increase, for example, the advanced warning capabilities of solar plasma storms [7]. More recently, the concept of E-sail formation flying has been proposed with the aim of redistributing the mission payload among multiple spacecraft and increasing the reference (characteristic) acceleration of each E-sail in the formation [10, 11, 12].

To simplify the mission analysis phase, an E-sail is often modelled as an ideal system, capable of providing a precise propulsive acceleration as a function of given attitude angles and tether voltage [13]. Such a requirement could hardly be met in practice for various reasons. First, the onboard sensing capabilities are limited, and a high accuracy actuation is very difficult, especially for an E-sail-based spacecraft with a small payload mass [14]. Second, due to the large flexible structure of a grid of thin and long tethers, the E-sail is vulnerable to different types of faults, such as attitude determination and control errors [15]. Third, the plasma properties of the solar wind are highly fluctuating and unpredictable, and often exhibit a chaotic behavior [16], thus giving rise to thrust amplitude uncertainties [17]. These involved problems necessitate the development of fault-tolerant control strategies that are able to compensate for the E-sail thrust errors.

In this respect, the aim of this paper is to present a distributed fault-tolerant control framework for E-sail relative motion at Sun-Earth artificial Lagrange points via local interaction only. A suitable potential function is incorporated in the control strategy, such that the relative distances among the E-sails evolve

within a limited range and synchronously converge to their desired values, while avoiding possible inter-sail collisions. Unlike the existing studies in which the communication topology of the E-sail relative motion is fixed and remains constant, the E-sail sensing capability is now uniquely determined by the relative distances in the formation and therefore admits a time-varying property, which is a more reasonable assumption in a realistic situation. In particular, a robust adaptive fault-tolerant consensus protocol is developed, capable of compensating unpredictable actuator uncertainties of the E-sails, thus extending the previous results in which only the formation tracking problem was considered [11].

This paper is organized as follows. The next section illustrates the generation of an AL_1 point by means of an E-sail, whose nominal plane is assumed to maintain a radial (that is, Sun-facing) orientation. Such AL_1 point is then taken as the reference point to derive the equations of relative motion and to develop an adaptive fault-tolerant control law aimed at guaranteeing consensus and collision avoidance in the presence of actuator failures. The proposed method is shown to be effective by means of an illustrative example. Some concluding remarks are finally included in the last section.

2. Problem formulation

2.1. Artificial Lagrange points with radial thrust

Consider the motion of an E-sail-based spacecraft S in a Sun-Earth circular restricted three-body system, described in a synodic reference frame $\mathcal{T}\,(O;\,\hat{\boldsymbol{x}},\hat{\boldsymbol{y}},\hat{\boldsymbol{z}})$; see Fig. 1. The origin O of $\mathcal{T}$ is located at the Sun-Earth's center-of-mass, the $(\hat{\boldsymbol{x}},\hat{\boldsymbol{y}})$ plane coincides with the ecliptic, the $\hat{\boldsymbol{x}}$ axis points to the Earth, and the $\hat{\boldsymbol{z}}$ axis is positive in the direction of the angular velocity vector $\boldsymbol{\omega}$. For convenience, the total mass of the primaries, the Sun-Earth distance, and the universal gravitational constant are all normalized to unity.

Denoting the O-S vector with $\boldsymbol{r}$, the E-sail equation of motion in the synodic reference frame can be written as [18]

$$\ddot{\boldsymbol{r}} + 2\,\boldsymbol{\omega}\times\dot{\boldsymbol{r}} = \frac{\partial\,\Omega}{\partial\,\boldsymbol{r}} + \boldsymbol{a} \tag{1}$$

where $\boldsymbol{a}$ is the propulsive acceleration vector, and Ω is a potential function defined as

$$\Omega \triangleq \frac{1}{2}\,(\boldsymbol{\omega}\times\boldsymbol{r})\cdot(\boldsymbol{\omega}\times\boldsymbol{r}) + \left(\frac{1-\mu}{r_\odot} + \frac{\mu}{r_\oplus}\right) \tag{2}$$

where μ is the normalized Earth's mass [18], while $r_\odot = \|\boldsymbol{r}_\odot\|$ and $r_\oplus = \|\boldsymbol{r}_\oplus\|$ are the Sun-spacecraft and the Earth-spacecraft distances, respectively. Using the recent thrust model by Huo et al. [19], according to which the E-sail shape is modelled as a rigid disk containing all of the tethers, the propulsive acceleration vector can be written in a compact, analytical, form as

$$\boldsymbol{a} = \frac{\beta\,(1-\mu)}{2\,r_\odot^2}\,[\boldsymbol{r}_\odot + (\boldsymbol{r}_\odot\cdot\hat{\boldsymbol{n}})\,\hat{\boldsymbol{n}}] \tag{3}$$

where $\hat{\boldsymbol{n}}$ is the unit vector normal to the sail nominal plane in the direction opposite to the Sun, and β is the lightness number defined as the ratio of the E-sail characteristic acceleration $a_\oplus$ to the solar gravitational acceleration at a reference distance $r = l \triangleq 1$ au, viz.

$$\beta \triangleq \frac{a_\oplus}{(1-\mu)/l^2} \tag{4}$$

In particular, the characteristic acceleration $a_\oplus$ is the maximum value of the propulsive acceleration magnitude $\|\boldsymbol{a}\|$ when $r = l$, while the normal unit vector $\hat{\boldsymbol{n}}$ can be written in terms of the classical sail attitude angles θ and ϕ (see Fig. 1) as

$$\hat{\boldsymbol{n}} = [\cos\,\theta\,\cos\,\phi,\ \cos\,\theta\,\sin\,\phi,\ \sin\,\theta]^{\mathrm{T}} \tag{5}$$

where $\theta \in [-\pi/2,\,\pi/2]$ rad is the angle between $\hat{\boldsymbol{n}}$ and the $(\hat{\boldsymbol{x}},\,\hat{\boldsymbol{y}})$ plane, and $\phi \in [-\pi/2,\,\pi/2]$ rad is the angle measured counterclockwise from $\hat{\boldsymbol{x}}$ to the projection of $\hat{\boldsymbol{n}}$ onto the $(\hat{\boldsymbol{x}},\,\hat{\boldsymbol{y}})$ plane.

In this paper, the artificial collinear points are obtained, as a function of the sail lightness number, with the assumption that the E-sail is subject to a purely radial thrust, that is, $\hat{\boldsymbol{a}} = \hat{\boldsymbol{r}}_\odot \equiv \hat{\boldsymbol{n}}$. The radial case is of particular interest since the sail attitude may be maintained in a passive way, so that the control

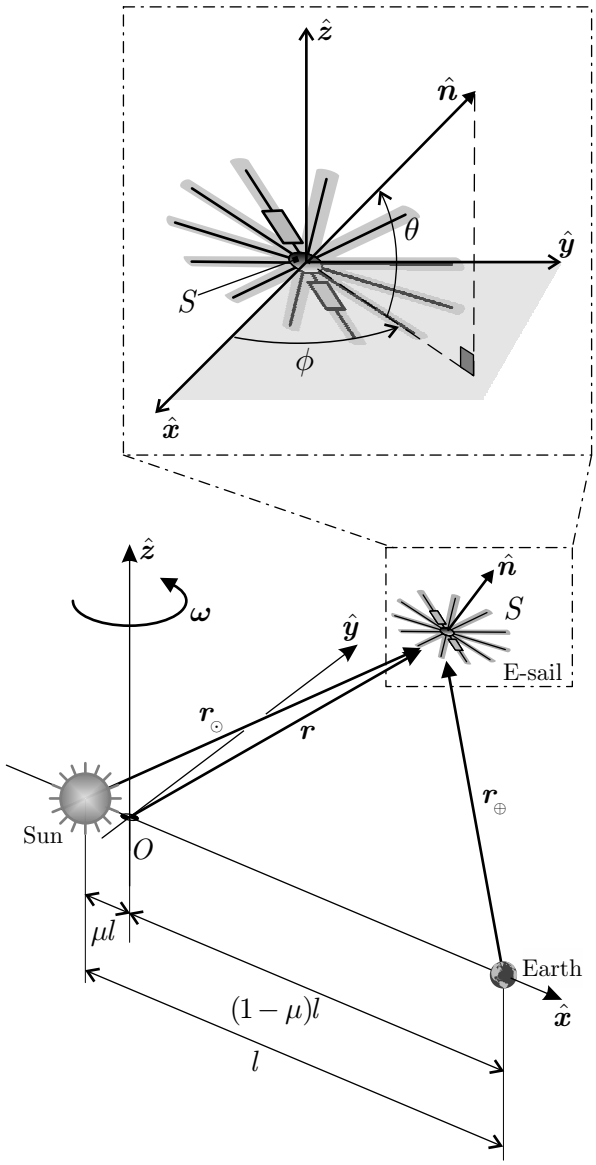

Figure 1: E-sail outline in a Sun-Earth circular restricted three-body system.

problem is significatively simplified [20]. The following analysis concentrates on artificial points around the first Lagrange point (referred to as AL_1 points), since the other artificial collinear points can be studied in a similar way.

In this context, consider an E-sail with a lightness number $\beta = \beta_0$, and select an AL_1 point on the $\hat{\boldsymbol{x}}$ axis (with a coordinate x_0) such that the conditions $\dot{\boldsymbol{r}} = \boldsymbol{0}_3$, $\ddot{\boldsymbol{r}} = \boldsymbol{0}_3$ and $\boldsymbol{r} = \boldsymbol{r}_0 = x_0\,\hat{\boldsymbol{x}}$ are met in Eq. (1). Accordingly, from Eqs. (1)–(3), it may be verified that x_0 satisfies the scalar equation

$$x_0 - \frac{1-\mu}{(x_0+\mu)^2} + \frac{\mu}{(x_0+\mu-1)^2} + \frac{\beta_0\,(1-\mu)}{x_0+\mu} = 0 \tag{6}$$

whose numerical solution $x_0 = x_0(\beta_0)$ is shown in Fig. 2. Note that the (axial) position of AL_1 shifts sunward as β_0 is increased.

2.2. E-Sail-based spacecraft relative motion

Assume now that a formation of $N \geq 3$ E-sail-based spacecraft moves in the vicinity of the reference AL_1 point of axial coordinate x_0. Note that such an AL_1 point does not necessarily coincide with the actual

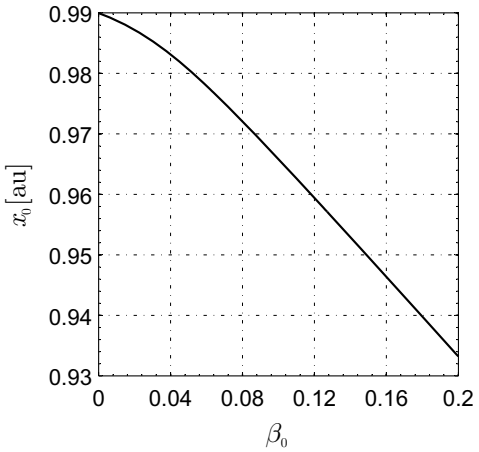

Figure 2: Location of AL_1 point as a function of the lightness number β_0.

position of a generic spacecraft in the formation.

Let $\boldsymbol{\rho}_i \triangleq \boldsymbol{r}_i - \boldsymbol{r}_0$ denote the position vector of the i-th spacecraft (subscript i) from the reference AL_1 point (subscript 0). Bearing in mind Eq. (1), the equation of relative motion in the synodic reference frame $\mathcal{T}$ can be written as

$$\ddot{\boldsymbol{\rho}}_i + 2\,\boldsymbol{\omega} \times \dot{\boldsymbol{\rho}}_i = \frac{\partial\,\Omega_i}{\partial\,\boldsymbol{r}_i} - \frac{\partial\,\Omega_0}{\partial\,\boldsymbol{r}_0} + \boldsymbol{a}_i - \boldsymbol{a}_0 \tag{7}$$

where $\boldsymbol{a}_0$ is the propulsive acceleration vector required to maintain the reference AL_1 point.

Taking into account that the relative distances $\|\boldsymbol{\rho}_i\|$ between each spacecraft in the formation structure and the reference AL_1 point is considerably smaller than the Sun-spacecraft distance, two terms in Eq. (7) can be linearized to first order as

$$\boldsymbol{a}_i \simeq \boldsymbol{a}_0 + \frac{\partial\,\boldsymbol{a}_0}{\partial\,\boldsymbol{r}_{\odot_0}}\,\boldsymbol{\rho}_i + \frac{\partial\,\boldsymbol{a}_0}{\partial\,[\theta_0,\ \phi_0]}\,[\Delta\,\theta_i,\ \Delta\,\phi_i]^{\mathrm{T}} + \frac{\partial\,\boldsymbol{a}_0}{\partial\,\beta_0}\,\Delta\,\beta_i \tag{8}$$

$$\frac{\partial\,\Omega_i}{\partial\,\boldsymbol{r}_i} \simeq \frac{\partial\,\Omega_0}{\partial\,\boldsymbol{r}_0} + \frac{\partial^2\,\Omega_0}{\partial\,\boldsymbol{r}_0^2}\,\boldsymbol{\rho}_i \tag{9}$$

where $\Delta\,\theta_i \triangleq \theta_i - \theta_0$ and $\Delta\,\phi_i \triangleq \phi_i - \phi_0$ are the relative attitude angles, $\Delta\,\beta_i \triangleq \beta_i - \beta_0$ is the relative lightness number, and the partial derivatives are

$$\frac{\partial\,\boldsymbol{a}_0}{\partial\,\boldsymbol{r}_{\odot_0}} = \frac{\beta_0\ (1-\mu)}{2\,r_{\odot_0}^2}\ \left[\hat{\boldsymbol{n}}_0\,\hat{\boldsymbol{n}}_0^{\mathrm{T}} - 2\,\hat{\boldsymbol{r}}_{\odot_0}\,\hat{\boldsymbol{r}}_{\odot_0}^{\mathrm{T}} - 2\ (\hat{\boldsymbol{r}}_{\odot_0} \cdot \hat{\boldsymbol{n}}_0)\left(\hat{\boldsymbol{n}}_0\,\hat{\boldsymbol{r}}_{\odot_0}^{\mathrm{T}}\right) + \mathbb{I}_3\right] \tag{10}$$

$$\frac{\partial\,\boldsymbol{a}_0}{\partial\,\beta_0} = \frac{(1-\mu)}{2\,r_{\odot_0}}\ [\hat{\boldsymbol{r}}_{\odot_0} + (\hat{\boldsymbol{r}}_{\odot_0} \cdot \hat{\boldsymbol{n}}_0)\ \hat{\boldsymbol{n}}_0] \tag{11}$$

$$\frac{\partial^2\,\Omega_0}{\partial\,\boldsymbol{r}_0^2} = \frac{(1-\mu)}{r_{\odot_0}^3}\ \left(3\,\hat{\boldsymbol{r}}_{\odot_0}\,\hat{\boldsymbol{r}}_{\odot_0}^{\mathrm{T}} - \mathbb{I}_3\right) + \frac{\mu}{r_{\oplus_0}^3}\ \left(3\,\hat{\boldsymbol{r}}_{\oplus_0}\,\hat{\boldsymbol{r}}_{\oplus_0}^{\mathrm{T}} - \mathbb{I}_3\right) + \mathrm{diag}\ (1,\ 1,\ 0) \tag{12}$$

$$\frac{\partial\,\boldsymbol{a}_0}{\partial\,[\theta_0,\ \phi_0]} = \frac{\partial\,\boldsymbol{a}_0}{\partial\,\hat{\boldsymbol{n}}_0}\,\frac{\partial\,\hat{\boldsymbol{n}}_0}{\partial\,[\theta_0,\,\phi_0]} \tag{13}$$

in which $\mathbb{I}_3 \in \mathbb{R}^{3\times 3}$ is the identity matrix, and

$$\frac{\partial\, \boldsymbol{a}_0}{\partial\, \hat{\boldsymbol{n}}_0} = \frac{\beta_0\ (1-\mu)}{2\, r_{\odot_0}}\ \left[\hat{\boldsymbol{n}}_0\, \hat{\boldsymbol{r}}^{\mathrm{T}}_{\odot_0} + (\hat{\boldsymbol{r}}_{\odot_0} \cdot \hat{\boldsymbol{n}}_0)\ \mathbb{I}_3\right] \tag{14}$$

$$\frac{\partial\, \hat{\boldsymbol{n}}_0}{\partial\, [\theta_0,\, \phi_0]} = \begin{bmatrix} -\sin\,\theta_0\,\cos\,\phi_0 & -\cos\,\theta_0\,\sin\,\phi_0 \\ -\sin\,\theta_0\,\sin\,\phi_0 & \cos\,\theta_0\,\cos\,\phi_0 \\ \cos\,\theta_0 & 0 \end{bmatrix} \tag{15}$$

In particular, since the reference AL_1 point is maintained assuming a Sun-facing orientation, the two attitude angles are $\theta_0 = \phi_0 = 0$, and $\hat{\boldsymbol{r}}_{\odot_0} \equiv \hat{\boldsymbol{n}}_0 = [1,\ 0,\ 0]^{\mathrm{T}}$. Finally, the linear differential equation of the spacecraft relative motion is obtained by substituting Eqs. (8)–(15) into Eq. (7), and the result is

$$\ddot{\boldsymbol{\rho}}_i + 2\, \mathbb{M}_v\, \dot{\boldsymbol{\rho}}_i + \mathbb{M}_p\, \boldsymbol{\rho}_i = \mathbb{M}_0\, \boldsymbol{u}_i \tag{16}$$

where $\boldsymbol{u}_i \triangleq [\Delta\,\theta_i,\ \Delta\,\phi_i,\ \Delta\,\beta_i]^{\mathrm{T}}$ denotes the control input vector of the i-th spacecraft, and the Δ symbol represents a variation with respect to the value required to maintain the reference AL_1 point, and the matrices

$$\mathbb{M}_v \triangleq \begin{bmatrix} 0 & -1 & 0 \\ 1 & 0 & 0 \\ 0 & 0 & 0 \end{bmatrix}, \quad \mathbb{M}_p \triangleq \mathrm{diag}\,(\mathbb{M}_{p_1},\ \mathbb{M}_{p_2},\ \mathbb{M}_{p_3}), \quad \mathbb{M}_0 \triangleq \frac{1-\mu}{2\ (x_0+\mu)} \begin{bmatrix} 0 & 0 & 2 \\ 0 & \beta_0 & 0 \\ \beta_0 & 0 & 0 \end{bmatrix} \tag{17}$$

in which

$$\mathbb{M}_{p_1} = -\frac{2\ (1-\mu)}{(x_0+\mu)^3} - \frac{2\,\mu}{(x_0+\mu-1)^3} + \frac{\beta_0\ (1-\mu)}{(x_0+\mu)^2} - 1, \quad \mathbb{M}_{p_2} = -\frac{\mathbb{M}_{p_1}+3}{2},$$

$$\mathbb{M}_{p_3} = -\frac{\mathbb{M}_{p_1}+1}{2} \tag{18}$$

In this context, the formation control is achieved by suitably adjusting the attitude angles and the lightness number of the E-sail.

3. Distributed fault-tolerant control

The relative motion of the spacecraft formation is now studied with the aim of obtaining a distributed collision-free dynamics based on a consensus control, which relies on a local information exchange between each vehicle of the formation structure. Consensus refers to a group of agents that will reach an agreement (or some common value) with a suitable control law by negotiating with their neighbors [21, 22]. In particular, bearing in mind basic concepts from graph theory, the information interaction is characterized by an undirected (bidirectional) topological graph in which the triplet $\mathcal{G} = (\mathcal{V}, \mathcal{E}, \mathbb{W})$ consists of a finite non-empty vertex set $\mathcal{V} \triangleq \{\upsilon_1, \ldots, \upsilon_N\}$, an edge set $\mathcal{E} \triangleq \{(\upsilon_1, \upsilon_2), \ldots, (\upsilon_{N-1}, \upsilon_N)\} \subseteq \mathcal{V} \times \mathcal{V}$, and a weighted (symmetric) adjacency matrix $\mathbb{W} = [w_{ij}] \in \mathbb{R}^{N\times N}$. In this context, a generic edge $(\upsilon_i, \upsilon_j) \in \mathcal{E}$ indicates a bidirectional path and the mutual transmission of state data between the vertices υ_i and υ_j. The generic entry of the weighted adjacency matrix $\mathbb{W}$ is $w_{ij} = w_{ji} > 0$, $\forall\ (\upsilon_j, \upsilon_i) \in \mathcal{E}$ with $i \neq j$, and $w_{ii} = 0$.

When modeling the communication topology of the spacecraft relative motion, each sail (or agent) is characterized by a vertex, while the data flow between any pair of E-sails is represented by a weighted edge. A collision avoidance in the presence of an actuator fault may be obtained with the aid of an artificial potential function embedded in a variable structure control, as is now discussed in detail.

3.1. Artificial potential function for collision avoidance

For an E-sail with a bulky flexible structure, comprised of a number of very long tethers (whose length may reach some kilometers), the possibility of inter-sail collisions is a serious hazard, which must be accounted for in the development phase of the control system. The problem is further complicated by the fact that a real-time knowledge of the actual formation topology is usually determined by the relative distances between the

agents. A possible communication link loss, due to a local drift in the relative motion between two agents, may therefore lead to a severe variation or even to a connectivity fail of the network topology. For this reason, it is meaningful to develop a collision-free control scheme for the relative motion, while keeping the network topology connected.

To this end, it is necessary to introduce first a potential function that is usually used in flocking (or swarm tracking) algorithms [23], whose aim is to ensure that the relative motion evolves within a prescribed safe region and eventually converges to its desired value $\delta_{ij}^{\star}$, viz.

$$\left\|\boldsymbol{\rho}_i-\boldsymbol{\rho}_j\right\| \in [\delta_{\min},\, \delta_{\max}] \quad \cap \quad \lim_{t\to+\infty}\left\|\boldsymbol{\rho}_i-\boldsymbol{\rho}_j\right\| = \delta_{ij}^{\star}, \qquad \forall\, (\upsilon_j,\upsilon_i)\in\mathcal{E} \tag{19}$$

where $\delta_{\max}$ is the maximum sensing (or communication) range and $\delta_{\min}$ is the minimum safe distance. The potential function V_{ij} for each pair of E-sails is defined as follows:

1) As long as $\left\|\boldsymbol{\rho}_i(0)-\boldsymbol{\rho}_j(0)\right\| \geq \delta_{\max}$, V_{ij} is a differentiable nonnegative function of $\left\|\boldsymbol{\rho}_i-\boldsymbol{\rho}_j\right\|$ such that
   i) V_{ij} is symmetric, that is, $V_{ij}=V_{ji}$, and $\partial V_{ij}/\partial \boldsymbol{\rho}_i = -\partial V_{ij}/\partial \boldsymbol{\rho}_j$;
   ii) V_{ij} arrives at its unique minimum when $\left\|\boldsymbol{\rho}_i-\boldsymbol{\rho}_j\right\|$ is equal to the desired value $\delta_{ij}^{\star}$, with $\max_{i,j}\,\delta_{ij}^{\star} \leq \delta_{\max}$;
   iii) $V_{ij}\to+\infty$ as $\left\|\boldsymbol{\rho}_i-\boldsymbol{\rho}_j\right\| \to \delta_{\min}$, with $\min_{i,j}\,\delta_{ij}^{\star} \geq \delta_{\min}$;
   iv) $\partial V_{ij}/\partial\left(\left\|\boldsymbol{\rho}_i-\boldsymbol{\rho}_j\right\|\right)=\mathbf{0}_3$ if $\left\|\boldsymbol{\rho}_i-\boldsymbol{\rho}_j\right\| \geq \delta_{\max}$;
   v) $V_{ii}\equiv c$, where $c\in\mathbb{R}^+$ is an arbitrary constant.

2) When, instead, $\left\|\boldsymbol{\rho}_i(0)-\boldsymbol{\rho}_j(0)\right\| < \delta_{\max}$, V_{ij} is defined as above with the only exception that condition iv) is replaced by $V_{ij}\to+\infty$ as $\left\|\boldsymbol{\rho}_i-\boldsymbol{\rho}_j\right\| \to \delta_{\max}$.

The connectivity maintenance mechanism of V_{ij} guarantees the persistent existence of the initial connectivity patterns of the topological graph $\mathcal{G}$. If $\mathcal{N}_i\subseteq\mathcal{V}$ denotes the neighbour set of the i-th spacecraft in the relative motion system, then $j\in\mathcal{N}_i(t)$ when $\left\|\boldsymbol{\rho}_i-\boldsymbol{\rho}_j\right\| \leq \delta_{\max}$ at time t, while $j\notin\mathcal{N}_i(t)$ otherwise. Note that the definition of V_{ij} admits the incorporation of a new vertex υ_j into the neighbor set $\mathcal{N}_i$ when $j\notin\mathcal{N}_i(t^-)$ and $j\in\mathcal{N}_i(t^+)$, $\forall\, j\in\mathcal{V}$. Accordingly, the initial topological graph $\mathcal{G}(0)$ is always a subgraph of $\mathcal{G}(t)$ for any $t>0$, i.e., $\mathcal{G}(0)\subseteq\mathcal{G}(t)$. In other words, the initial edge in the graph will never be lost when using such an artificial potential function.

For illustrative purposes, two different artificial potential functions, $V_{ij}^{(1)}$ and $V_{ij}^{(2)}$, are now compared. Their derivatives are given by

$$\frac{\partial V_{ij}^{(1)}}{\partial \boldsymbol{\rho}_i} = \begin{cases} \mathbf{0}_3 & \text{if} \quad \left\|\boldsymbol{\rho}_i-\boldsymbol{\rho}_j\right\| > \delta_{\max} \\ \dfrac{\boldsymbol{\rho}_i-\boldsymbol{\rho}_j}{\left\|\boldsymbol{\rho}_i-\boldsymbol{\rho}_j\right\|}\cos\left[\dfrac{\pi}{\delta_{\max}-\delta_{ij}^{\star}}\left(\left\|\boldsymbol{\rho}_i-\boldsymbol{\rho}_j\right\|-\dfrac{\delta_{\max}+\delta_{ij}^{\star}}{2}\right)\right] & \text{if} \quad \delta_{ij}^{\star} < \left\|\boldsymbol{\rho}_i-\boldsymbol{\rho}_j\right\| \leq \delta_{\max} \\ \dfrac{\boldsymbol{\rho}_i-\boldsymbol{\rho}_j}{\left\|\boldsymbol{\rho}_i-\boldsymbol{\rho}_j\right\|}\dfrac{\left\|\boldsymbol{\rho}_i-\boldsymbol{\rho}_j\right\|-\delta_{ij}^{\star}}{\left\|\boldsymbol{\rho}_i-\boldsymbol{\rho}_j\right\|-\delta_{\min}} & \text{if} \quad \delta_{\min} < \left\|\boldsymbol{\rho}_i-\boldsymbol{\rho}_j\right\| \leq \delta_{ij}^{\star} \end{cases} \tag{20}$$

$$\frac{\partial V_{ij}^{(2)}}{\partial \boldsymbol{\rho}_i} = \begin{cases} \dfrac{\boldsymbol{\rho}_i-\boldsymbol{\rho}_j}{\left\|\boldsymbol{\rho}_i-\boldsymbol{\rho}_j\right\|}\dfrac{\left\|\boldsymbol{\rho}_i-\boldsymbol{\rho}_j\right\|-\delta_{ij}^{\star}}{\left(\left\|\boldsymbol{\rho}_i-\boldsymbol{\rho}_j\right\|-\delta_{\max}\right)^2} & \text{if} \quad \delta_{ij}^{\star} < \left\|\boldsymbol{\rho}_i-\boldsymbol{\rho}_j\right\| \leq \delta_{\max} \\ \dfrac{\boldsymbol{\rho}_i-\boldsymbol{\rho}_j}{\left\|\boldsymbol{\rho}_i-\boldsymbol{\rho}_j\right\|}\dfrac{\left\|\boldsymbol{\rho}_i-\boldsymbol{\rho}_j\right\|-\delta_{ij}^{\star}}{\left\|\boldsymbol{\rho}_i-\boldsymbol{\rho}_j\right\|-\delta_{\min}} & \text{if} \quad \delta_{\min} < \left\|\boldsymbol{\rho}_i-\boldsymbol{\rho}_j\right\| \leq \delta_{ij}^{\star} \end{cases} \tag{21}$$

A possible way to guarantee that the initially existing network patterns never collapse for any $t>0$, is choosing the artificial potential function to coincide with $V_{ij}^{(1)}$ if $\left\|\boldsymbol{\rho}_i(0)-\boldsymbol{\rho}_j(0)\right\| \geq \delta_{\max}$ and with $V_{ij}^{(2)}$ otherwise, as is suggested in Ref. [23]. An example of the artificial potential functions $V_{ij}^{(1)}$ and $V_{ij}^{(2)}$ is shown in Fig. 3, in which the desired spacecraft relative distance is $\delta_{ij}^{\star}=80\,\text{km}$, the maximum sensing radius is $\delta_{\max}=100\,\text{km}$, and the minimum safe distance is $\delta_{\min}=50\,\text{km}$.

3.2. Inclusion of E-sail actuator fault

Equation (3) provides a thrust model of an ideal E-sail, in which the attitude angles $\{\theta,\phi\}$ and the lightness number β are the control variables. By virtue of the previously defined artificial potential function

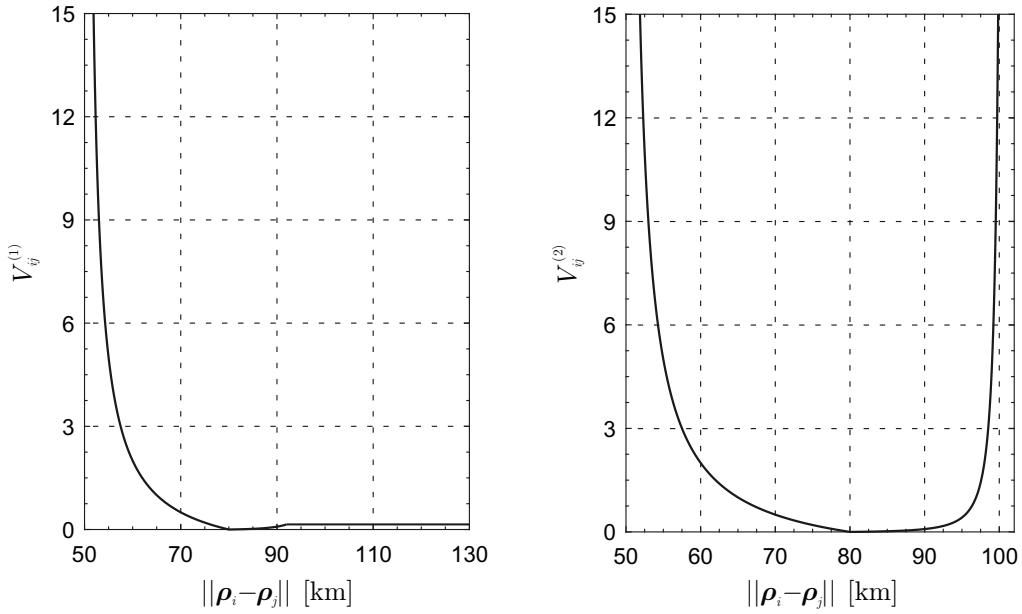

(a) Potential function $V_{ij}^{(1)}$ (b) Potential function $V_{ij}^{(2)}$

Figure 3: Potential functions $V_{ij}^{(1)}$ and $V_{ij}^{(2)}$ with $\delta_{\max} = 100$ km, $\delta_{\min} = 50$ km, and $\delta_{ij}^{\star} = 80$ km.

V_{ij}, the basic consensus-based algorithm [24] is given by

$$\boldsymbol{u}_i = \mathbb{M}_0^{-1} \left[2\,\mathbb{M}_v\,\dot{\boldsymbol{\rho}}_i + \mathbb{M}_p\,\boldsymbol{\rho}_i - \sum_{j\in\mathcal{N}_i} w_{ij}\,\left(\dot{\boldsymbol{\rho}}_i - \dot{\boldsymbol{\rho}}_j\right) - \sum_{j\in\mathcal{N}_i} \frac{\partial\, V_{ij}}{\partial\, \boldsymbol{\rho}_i} \right] \tag{22}$$

Using the candidate Lyapunov function [24]

$$V = \frac{1}{2}\sum_{i=1}^{N} \boldsymbol{\rho}_i^{\mathrm{T}}\,\boldsymbol{\rho}_i + \frac{1}{2}\sum_{i=1}^{N}\sum_{j\in\mathcal{N}_i} V_{ij} \tag{23}$$

The distributed control law represented by (22) has been proved well suited to the multi-agent system with ideal actuators (without fault).

In practice, however, an E-sail-based spacecraft is subjected to unpredictable position errors when immersed in a fluctuating solar wind environment [17], and it may also suffer from attitude control errors, which would induce a discrepancy between the actual control command $\tilde{\boldsymbol{u}}_i$ and its required (nominal) value $\boldsymbol{u}_i$. In that case, the actual output including the actuator fault of the i-th spacecraft can be modeled as [25, 26]

$$\tilde{\boldsymbol{u}}_i = \mathbb{H}_i\,\boldsymbol{u}_i + \boldsymbol{\epsilon}_i \tag{24}$$

where the healthy indicator matrix $\mathbb{H}_i \triangleq \mathrm{diag}\,(\mathbb{H}_{\theta_i},\, \mathbb{H}_{\phi_i},\, \mathbb{H}_{\beta_i}) \in (\mathbb{O}_3,\, \mathbb{I}_3]$ reflects the loss of actuator effectiveness, and $\mathbb{O}_3 \in \mathbb{R}^{3\times 3}$ is the zero matrix. The unknown bias fault $\boldsymbol{\epsilon}_i$ of the control input is defined as $\boldsymbol{\epsilon}_i \triangleq [\epsilon_{\theta_i},\, \epsilon_{\phi_i},\, \epsilon_{\beta_i}]^{\mathrm{T}}$. The various types of actuator faults [26] are summarized in Table 1.

Without loss of generality, the effectiveness loss and bias fault will be both considered in the following analysis, i.e. $\mathbb{H}_i \in (\mathbb{O}_3,\, \mathbb{I}_3]$ and $\boldsymbol{\epsilon}_i \neq \mathbf{0}_3$. Accordingly, Eq. (16) can be slightly modified to adapt the E-sail relative dynamics in the presence of an actuator fault as

$$\ddot{\boldsymbol{\rho}}_i + 2\,\mathbb{M}_v\,\dot{\boldsymbol{\rho}}_i + \mathbb{M}_p\,\boldsymbol{\rho}_i = \mathbb{M}_0\,\mathbb{H}_i\,\boldsymbol{u}_i + \mathbb{M}_0\,\boldsymbol{\epsilon}_i \tag{25}$$

The uncertain part of the actuator fault in Eq. (25) is assumed to be bounded and such that $\|\mathbb{M}_0\,\boldsymbol{\epsilon}_i\| \leq \xi_{i1}$, where $\xi_{i1} \in \mathbb{R}^{+}$ is an unknown parameter.

Table 1: Types of actuator faults

Type	$\mathbb{H}_i$	$\boldsymbol{\epsilon}_i$
Healthy	$\mathbb{I}_3$	$\mathbf{0}_3$
Effectiveness loss	$(\mathbb{O}_3,\, \mathbb{I}_3)$	$\mathbf{0}_3$
Bias	$\mathbb{I}_3$	$\neq \mathbf{0}_3$
Effectiveness loss & bias	$(\mathbb{O}_3,\, \mathbb{I}_3)$	$\neq \mathbf{0}_3$

A distributed control strategy involving an adaptive parameter updating scheme will now be designed for the relative motion system described by Eq. (25), in such a way that an autonomous collision-free consensus is obtained even in the presence of an E-sail actuator fault. To proceed, first introduce the auxiliary variable

$$\boldsymbol{s}_i \triangleq \dot{\boldsymbol{\rho}}_i + \sigma \sum_{j\in\mathcal{N}_i} \frac{\partial\, V_{ij}}{\partial\, \boldsymbol{\rho}_i} \tag{26}$$

where $\sigma \in \mathbb{R}^+$, and the low-pass filter

$$\varepsilon_i\, \dot{\boldsymbol{\chi}}_i = -\boldsymbol{\chi}_i + \sigma \sum_{j\in\mathcal{N}_i} \frac{\partial\, V_{ij}}{\partial\, \boldsymbol{\rho}_i} \tag{27}$$

whose bandwidth is $\varepsilon_i \in \mathbb{R}^+$. Equation (27) suggests that if ε_i is a very small quantity, then $\sigma \sum_{j\in\mathcal{N}_i} \partial\, V_{ij}/\partial\, \boldsymbol{\rho}_i \simeq \boldsymbol{\chi}_i$. In addition, since $\left\| \sum_{j\in\mathcal{N}_i} \partial\, V_{ij}/\partial\, \boldsymbol{\rho}_i \right\|$ is bounded, it is reasonable to assume that $\left\| \sigma\, \frac{\mathrm{d}}{\mathrm{d}\, t} \left(\sum_{j\in\mathcal{N}_i} \frac{\partial\, V_{ij}}{\partial\, \boldsymbol{\rho}_i} \right) \right\| \simeq \|\dot{\boldsymbol{\chi}}_i\| \leq \xi_{i2}$ when $\varepsilon_i \ll 1$, where $\xi_{i2} \in \mathbb{R}^+$ is the unknown parameter. In principle, ξ_{i2} may be found once the potential function V_{ij} is fixed, however elaborate mathematical manipulations are often necessary when the expression of V_{ij} is involved. Therefore, the unknown parameter ξ_{i2} is obtained through a low-pass filter rather than using an analytical approach.

The distributed fault-tolerant control protocol, used for an E-sail collision-free motion described by Eq. (25), is proposed in the form

$$\boldsymbol{u}_i = (\mathbb{M}_0\, \mathbb{H}_i)^{-1} \left[-\sum_{k=1}^{2} \hat{\xi}_{ik}\, \mathrm{sign}\,(\boldsymbol{s}_i) - \mathbb{K}_i\, \boldsymbol{s}_i - \|2\, \mathbb{M}_v\, \dot{\boldsymbol{\rho}}_i + \mathbb{M}_p\, \boldsymbol{\rho}_i\|\, \mathrm{sign}\,(\boldsymbol{s}_i) \right] \tag{28}$$

where $\mathbb{K}_i \in \mathbb{R}^{3\times 3}$ is a symmetric positive definite matrix, and $\hat{\xi}_{ik}$ is the estimated value of ξ_{ik}. Because $\hat{\xi}_{ik}$ is not known a priori, an adaptive parameter updating law is designed in the form

$$\dot{\hat{\xi}}_{ik} = -\gamma_{ik}^2\, \hat{\xi}_{ik} + \eta_{ik}\, \|\boldsymbol{s}_i\| \tag{29}$$

$$\dot{\gamma}_{ik} = -\kappa_{ik}\, \gamma_{ik} \tag{30}$$

where $\{\eta_{ik}, \kappa_{ik}\} \in \mathbb{R}^+$ with $k = 1, 2$. The control strategy is a consequence of the following theorem.

Theorem 1: Assume that the topological graph $\mathcal{G}$ characterizing the E-sail relative motion is initially connected, and that the relative distance between any pair of E-sails is beyond the safe region, i.e., $\left\|\boldsymbol{\rho}_i(0) - \boldsymbol{\rho}_j(0)\right\| > \delta_{\min}$. Using the control law given by Eqs. (26)–(30), the E-sail relative distances ultimately converge to their local minima and any inter-sail collision is avoided as long as $\mathbb{K}_i - \frac{1}{4}\, \mathbb{I}_3 > \mathbb{O}_3$, with $i = 1, \ldots, N$.

Proof: Consider the candidate Lyapunov function:

$$V = \sigma \sum_{i=1}^{N} \sum_{j\in\mathcal{N}_i} V_{ij} + \sum_{i=1}^{N} \frac{1}{2}\, \boldsymbol{s}_i^{\mathrm{T}}\, \boldsymbol{s}_i + \sum_{i=1}^{N} \sum_{k=1}^{2} \left[\frac{\left(\xi_{ik} - \hat{\xi}_{ik}\right)^2}{2\, \eta_{ik}} + \frac{\gamma_{ik}^2\, \xi_{ik}^2}{8\, \kappa_{ik}\, \eta_{ik}} \right] \tag{31}$$

Substituting Eqs. (25)–(30) into Eq. (31), the derivative of V is

$$\begin{aligned}\dot{V} = \sigma \sum_{i=1}^{N} \sum_{j\in\mathcal{N}_i} \dot{V}_{ij} + \sum_{i=1}^{N} \boldsymbol{s}_i^{\mathrm{T}} \Bigg[& -2\,\mathbb{M}_v\,\dot{\boldsymbol{\rho}}_i - \mathbb{M}_p\,\boldsymbol{\rho}_i + (\mathbb{M}_0\,\boldsymbol{\epsilon}_i + \boldsymbol{d}_i) + \sigma\,\frac{\mathrm{d}}{\mathrm{d}\,t}\left(\sum_{j\in\mathcal{N}_i} \frac{\partial\,V_{ij}}{\partial\,\boldsymbol{\rho}_i}\right) \\ & - \sum_{k=1}^{2} \hat{\xi}_{ik}\,\mathrm{sign}\,(\boldsymbol{s}_i) - \mathbb{K}_i\,\boldsymbol{s}_i \;\; - \|2\,\mathbb{M}_v\,\dot{\boldsymbol{\rho}}_i + \mathbb{M}_p\,\boldsymbol{\rho}_i\|\;\mathrm{sign}\,(\boldsymbol{s}_i)\Bigg] \\ & + \sum_{i=1}^{N}\sum_{k=1}^{2}\left[\frac{\xi_{ik}-\hat{\xi}_{ik}}{\eta_{ik}}\left(\gamma_{ik}^2\,\hat{\xi}_{ik} - \eta_{ik}\;\|\boldsymbol{s}_i\|\right) - \frac{\gamma_{ik}^2\,\xi_{ik}^2}{4\,\eta_{ik}}\right]\end{aligned} \tag{32}$$

After some algebraic manipulations, it can be verified that

$$\dot{V} \leq \sigma \sum_{i=1}^{N} \sum_{j\in\mathcal{N}_i} \dot{V}_{ij} - \sum_{i=1}^{N} \boldsymbol{s}_i^{\mathrm{T}}\,\mathbb{K}_i\,\boldsymbol{s}_i \tag{33}$$

From Eq. (26), the following relationship holds

$$\begin{aligned}\sigma \sum_{i=1}^{N} \sum_{j\in\mathcal{N}_i} \dot{V}_{ij} &= \sigma \sum_{i=1}^{N} \sum_{j\in\mathcal{N}_i} \frac{\partial\,V_{ij}}{\partial\,\boldsymbol{\rho}_i}\,\dot{\boldsymbol{\rho}}_i \\ &= \sum_{i=1}^{N}\left[\sigma \sum_{j\in\mathcal{N}_i} \frac{\partial\,V_{ij}}{\partial\,\boldsymbol{\rho}_i}\left(\boldsymbol{s}_i - \sigma \sum_{j\in\mathcal{N}_i} \frac{\partial\,V_{ij}}{\partial\,\boldsymbol{\rho}_i}\right)\right]\end{aligned} \tag{34}$$

Let $\boldsymbol{q}_i \triangleq \sum_{j\in\mathcal{N}_i} \frac{\partial\,V_{ij}}{\partial\,\boldsymbol{\rho}_i}$, and observe that with the aid of Eq. (34), Eq. (33) can be rewritten in the form

$$\begin{aligned}\dot{V} &\leq \sum_{i=1}^{N} \left[\sigma\,\boldsymbol{q}_i^{\mathrm{T}}\;(\boldsymbol{s}_i - \sigma\,\boldsymbol{q}_i)\right] - \sum_{i=1}^{N} \boldsymbol{s}_i^{\mathrm{T}}\,\mathbb{K}_i\,\boldsymbol{s}_i \\ &= -\left[\boldsymbol{s}^{\mathrm{T}},\;\boldsymbol{q}^{\mathrm{T}}\right] \begin{bmatrix} \mathbb{K} & -\frac{\sigma}{2}\,\mathbb{I}_{3N} \\ -\frac{\sigma}{2}\,\mathbb{I}_{3N} & \sigma^2\,\mathbb{I}_{3N} \end{bmatrix} \left[\boldsymbol{s}^{\mathrm{T}},\;\boldsymbol{q}^{\mathrm{T}}\right]^{\mathrm{T}}\end{aligned} \tag{35}$$

where $\boldsymbol{q} \triangleq [\boldsymbol{q}_1^{\mathrm{T}}, \ldots, \boldsymbol{q}_N^{\mathrm{T}}]^{\mathrm{T}}$, $\boldsymbol{s} \triangleq [\boldsymbol{s}_1^{\mathrm{T}}, \ldots, \boldsymbol{s}_N^{\mathrm{T}}]^{\mathrm{T}}$, and $\mathbb{K} \triangleq \mathrm{diag}\,(\mathbb{K}_1, \ldots, \mathbb{K}_N)$. From Eq. (35), it follows that $\dot{V} \leq 0$ if $\mathbb{K}_i - \frac{1}{4}\,\mathbb{I}_3 > \mathbb{O}_3$.

Note that $V > 0$ and $\dot{V} \leq 0$, hence $\{V_{ij}, \boldsymbol{s}_i\} \in \mathcal{L}_\infty$. Because V_{ij} is bounded, a possible collision may occur only when $V_{ij} \to +\infty$. This means that the inter-sail collision avoidance is guaranteed, i.e., $\left\|\boldsymbol{\rho}_i - \boldsymbol{\rho}_j\right\| > \delta_{\min}$, $\forall\, t \geq 0$. It can also be verified that $\ddot{V} \in \mathcal{L}_\infty$ and $\dot{V}$ is uniformly continuous. From Barbalat's lemma [27], we get $\dot{V} \to 0$ as $t \to +\infty$, and hence, according to Eq. (35), $\boldsymbol{s}_i \to \boldsymbol{0}_3$ and $\boldsymbol{q}_i \to \boldsymbol{0}_3$. From the definitions of $\boldsymbol{q}_i$ and V_{ij}, it can be concluded that the potential function V_{ij} converges to its local minimum, which amounts to stating that $\left\|\boldsymbol{\rho}_i - \boldsymbol{\rho}_j\right\| \to \delta_{ij}^{\star}$. $\square$

4. Mission application

A mission scenario consisting of four E-sail-based spacecraft (i.e. $N = 4$), moving around a reference AL_1 point placed at $x_0 = 0.966$, is now analyzed to illustrate the performance of the proposed distributed fault-tolerant control system. In particular, according to Eq. (6) the lightness number required to maintain the reference AL_1 point is $\beta_0 = 0.1$. The potential functions used for connectivity maintenance and collision avoidance are described by Eqs. (20)–(21) and reported in Fig. 3. The desired relative distance among the E-sails is $\delta_{ij}^{\star} = 80\,\mathrm{km}$, the maximum sensing radius of each E-sail is $\delta_{\max} = 100\,\mathrm{km}$, and the minimum safe distance is $\delta_{\min} = 50\,\mathrm{km}$. The initial relative positions of the four E-sails with respect to the reference AL_1 point are $\boldsymbol{\rho}_1\,(0) = [10,\ 35,\ 37]^{\mathrm{T}}$ km, $\boldsymbol{\rho}_2\,(0) = [-10,\ -36,\ 38]^{\mathrm{T}}$ km, $\boldsymbol{\rho}_3\,(0) = [-10,\ 37,\ -37]^{\mathrm{T}}$ km,

$\boldsymbol{\rho}_4(0) = [10,\ -36,\ -35]^{\mathrm{T}}$ km, and the initial relative velocities are assumed to be zero, i.e. $\dot{\boldsymbol{\rho}}_i(0) = \mathbf{0}_3$. It can be verified that, with these initial conditions, the initial edge set of the E-sail relative motion is $\mathcal{E}(0) = \{(\upsilon_1, \upsilon_2), (\upsilon_1, \upsilon_3), (\upsilon_2, \upsilon_4), (\upsilon_3, \upsilon_4)\}$, which implies a connected communication topology.

In the numerical simulations, the dimensionless parameter in Eq. (26) is chosen as $\sigma = 10^{-4}$, and the feedback gain matrix in Eq. (28) is $\mathbb{K}_i = 100\,\mathbb{I}_3$. The parameters η_{ik} and κ_{ik} in Eqs. (29)–(30) are $\eta_{ik} = 0.8$ and $\kappa_{ik} = 1$, while the initial estimations of $\hat{\xi}_{ik}$ and γ_{ik} are $\hat{\xi}_{ik}(0) = 10^{-6}$ and $\gamma_{ik}(0) = 10^{-3}$, respectively. Assume that only 60% of the required control input can be provided by the actuator of each spacecraft, that is, the healthy indicator matrix $\mathbb{H}_i = 0.6\,\mathbb{I}_3$, and the actuator bias fault $\boldsymbol{\epsilon}_i$ randomly fluctuates within a small cubic space, i.e. $\left\{\boldsymbol{\epsilon}_i \mid \boldsymbol{\epsilon}_i \in \left[-10^{-3},\, 10^{-3}\right]^2 \text{ deg} \times \left[-10^{-5},\, 10^{-5}\right]\right\}$. In addition, all external perturbations such as Earth's oblateness and lunar attraction are not taken into account, because the magnitude of their induced acceleration is of fourth or higher order.

The instantaneous positions at $t = \{0;\, 6\}$ day of the four E-sails are illustrated in Fig. 4, showing that the developed control law given by Eqs. (26)–(30) allows the four E-sails to be perfectly synchronized with negligible final errors. When there exists a communication link (solid line in Fig. 4) between the i-th and j-th E-sail, i.e., $\forall\,(\upsilon_j, \upsilon_i) \in \mathcal{E}$, the time histories of the relative distances are given in Fig. 5, in which the relative distance $\left\|\boldsymbol{\rho}_i - \boldsymbol{\rho}_j\right\|$ successfully converges to the desired values $\delta_{ij}^{\star}$ within about 6 days. By contrast, neither a communication link exists (dashed line in Fig. 4) between the 1-st and 4-th E-sail nor the 2-nd and 3-rd E-sail during the whole process, i.e. $(\upsilon_1, \upsilon_4) \notin \mathcal{E}(t) \cap (\upsilon_2, \upsilon_3) \notin \mathcal{E}(t)$, $\forall\, t > 0$, therefore, the relative distances $\|\boldsymbol{\rho}_1 - \boldsymbol{\rho}_4\|$ and $\|\boldsymbol{\rho}_2 - \boldsymbol{\rho}_3\|$ finally tend to some possible values within the range $\left(\delta_{\max},\, 2\,\delta_{ij}^{\star}\right)$, as is confirmed by Fig. 6. In fact, the lower bound $\delta_{\max}$ and upper bound $2\,\delta_{ij}^{\star}$ is naturally determined by the artificial potential function V_{ij} designed in Eqs. (20)–(21). Fig. 7 reports the corresponding E-sail velocities $\dot{\boldsymbol{\rho}}_i$ between any pair of E-sails for a time span of 6 days, implying that all of the E-sail velocities gradually tend to zero at the same speed. Note that the initial connectivity patten is well maintained, and no edge is lost during the transition phase. The control input $\boldsymbol{u}_i$ of each E-sail is illustrated in Fig. 8. Despite the intrinsic chattering phenomenon due to the variable structure control, the consensus-based distributed architecture is able to achieve a collision-free coordination for the E-sail relative motion in the presence of actuator errors.

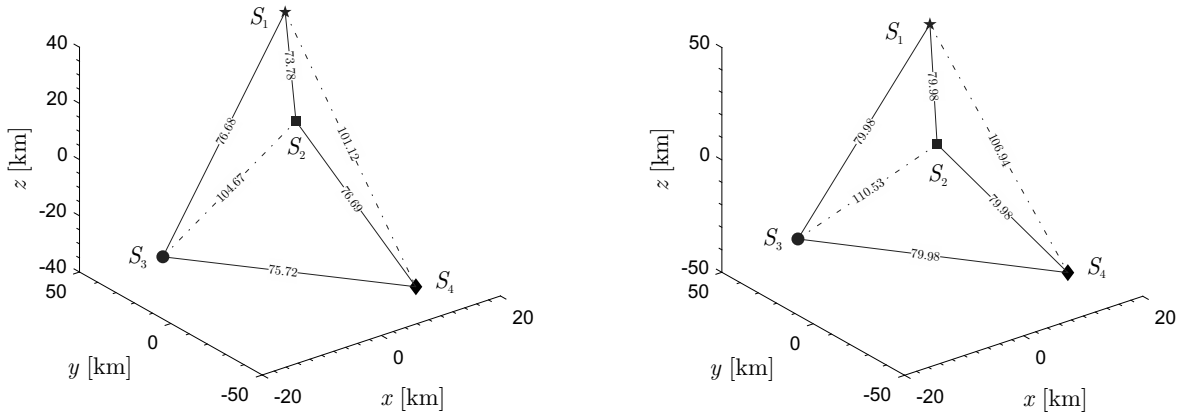

(a) $t = 0$ day (b) $t = 6$ day

Figure 4: Initial and final configurations of four E-sails.

Because the fault-tolerant control system in Eq. (28) is distributed and behavior-based, a stable E-sail relative motion with a tetrahedron configuration is expected to turn out in a self-organized way. In particular, when the number of E-sail increases, different types of spatial configurations such as Bravais lattices are likely to occur, as is discussed in Ref. [28].

For comparison, consider now the ideal case in which the actuator of an E-sail-based spacecraft is fully functional. In this case, the healthy indicator matrix $\mathbb{H}_i = \mathbb{I}_3$, and the bias fault $\boldsymbol{\epsilon} = \mathbf{0}_3$, see Table 1. The control law represented by Eq. (22) for the ideal case is thus accordance with that of the degenerated form in the presence of actuator fault, see Eq. (28). The relative distances between each pair of E-sails are illustrated in Fig. 9, while the required control input $\boldsymbol{u}_i$ is shown in Fig. 10. In contrast with the results

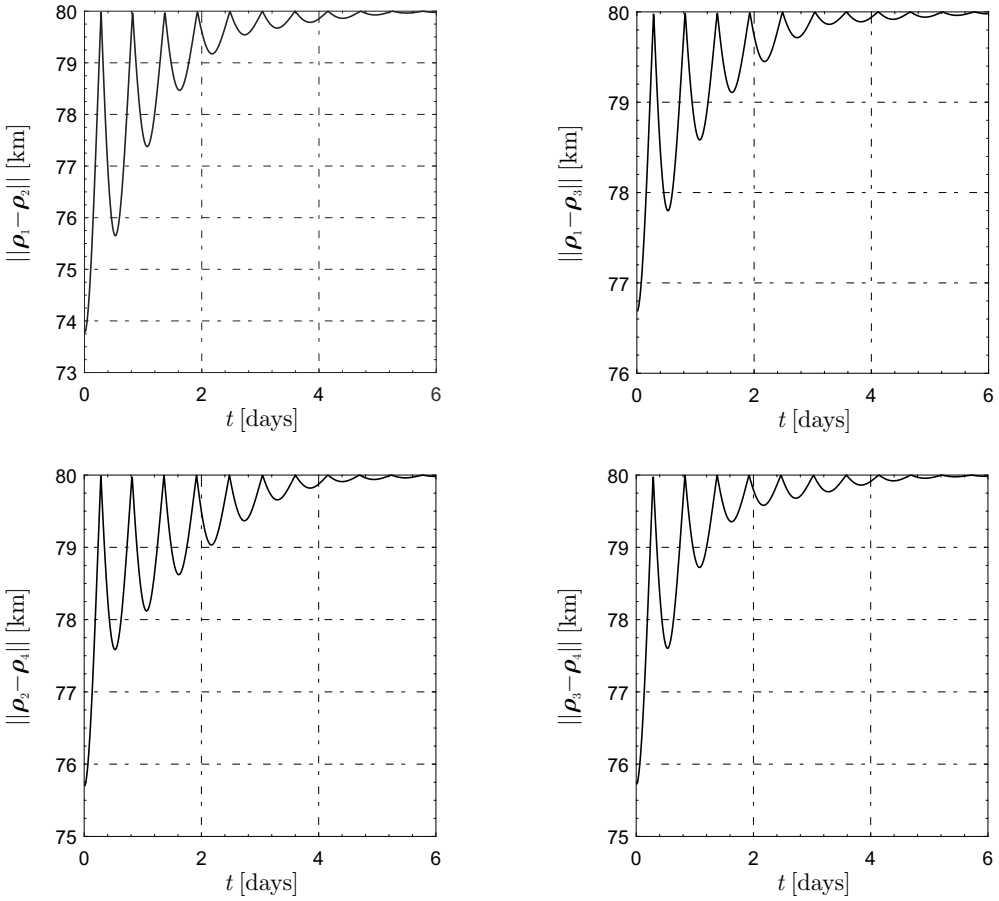

Figure 5: Relative distances with actuator fault for $(\upsilon_j, \upsilon_i) \in \mathcal{E}\ (t)$.

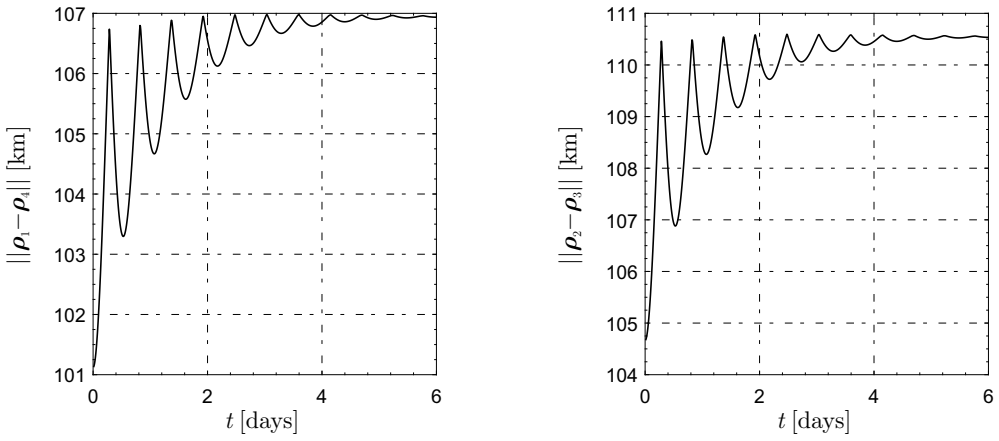

Figure 6: Relative distances with actuator fault for $(\upsilon_j, \upsilon_i) \notin \mathcal{E}\,(t)$.

given by Figs. 5–8, the control law given by Eq. (22) with an ideal actuator allows a faster convergence rate and negligible steady errors.

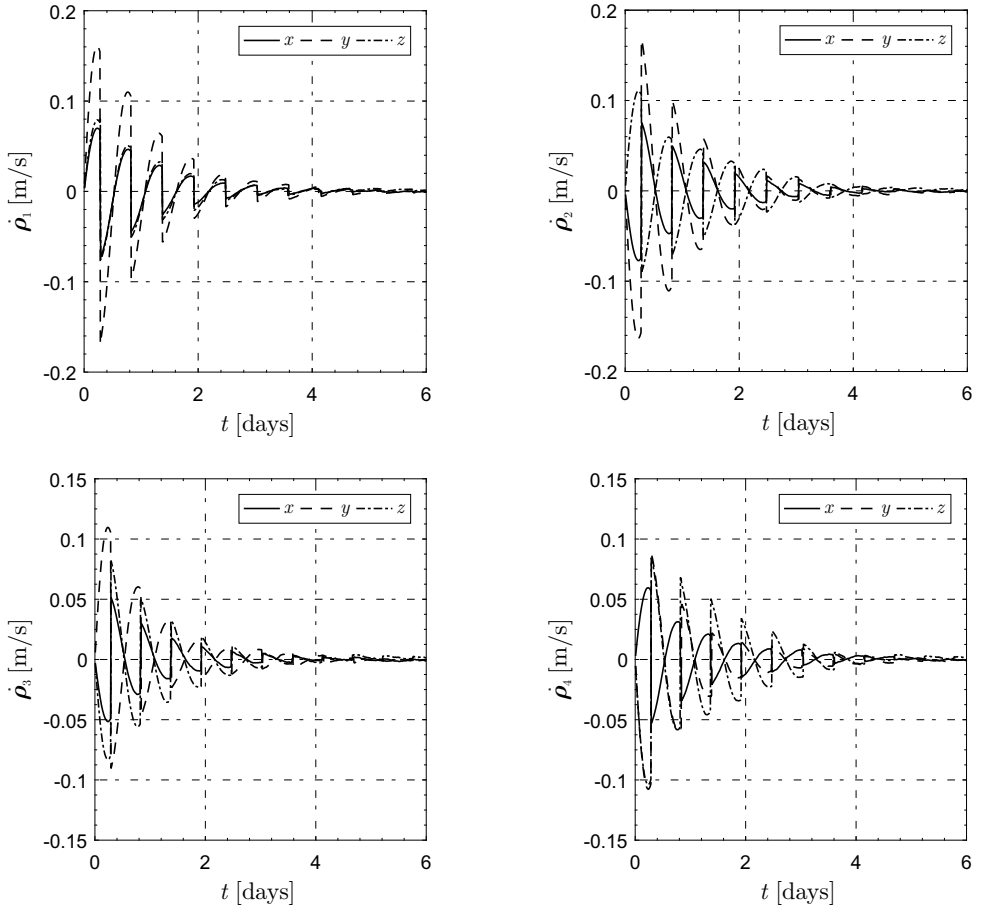

Figure 7: Velocity variations of a four-sail formation.

5. Conclusions

In this paper, the problem of E-sail relative motion around artificial (collinear) Lagrange points has been investigated. A distributed fault-tolerant control scheme, relying on a consensus protocol that exploits local measurable information only, has been developed to account for unpredictable E-sail actuator fault. In particular, the artificial potential functions comprised of a connectivity maintenance mechanism have been designed in a proper way, such that the E-sail relative distances converge to their desired values, while the inter-sail collision avoidance is guaranteed. The well-defined potential functions allow a time-varying information exchange topology that is uniquely determined by the relative distances among the E-sails.

Illustrative examples have shown that the fault-tolerant control strategy enables consensus for E-sail relative motion around artificial Lagrange points, despite of a more oscillating behavior compared with that in the ideal case. The proposed method facilitates the design of future advanced formation missions that involve, for instance, a swarm of E-sails in the presence of a strongly fluctuating solar wind environment.

In theory, some unfavorable circumstances could arise, for example, when one E-sail is just behind another along the solar wind propagation direction. In that case, the rear E-sail would be in the plasma wake of the other one, and the thrust necessary for relative motion control would be unavailable. That kind of problem, however, has not been considered in this paper, since such a situation might occur along very limited time intervals only. A natural extension of this work is the study of consensus protocols in the presence of more practical constraints, when very-large-distance cluster missions are considered. In those cases, other problems such as time delays should be taken into account by suitably designing the overall control scheme.

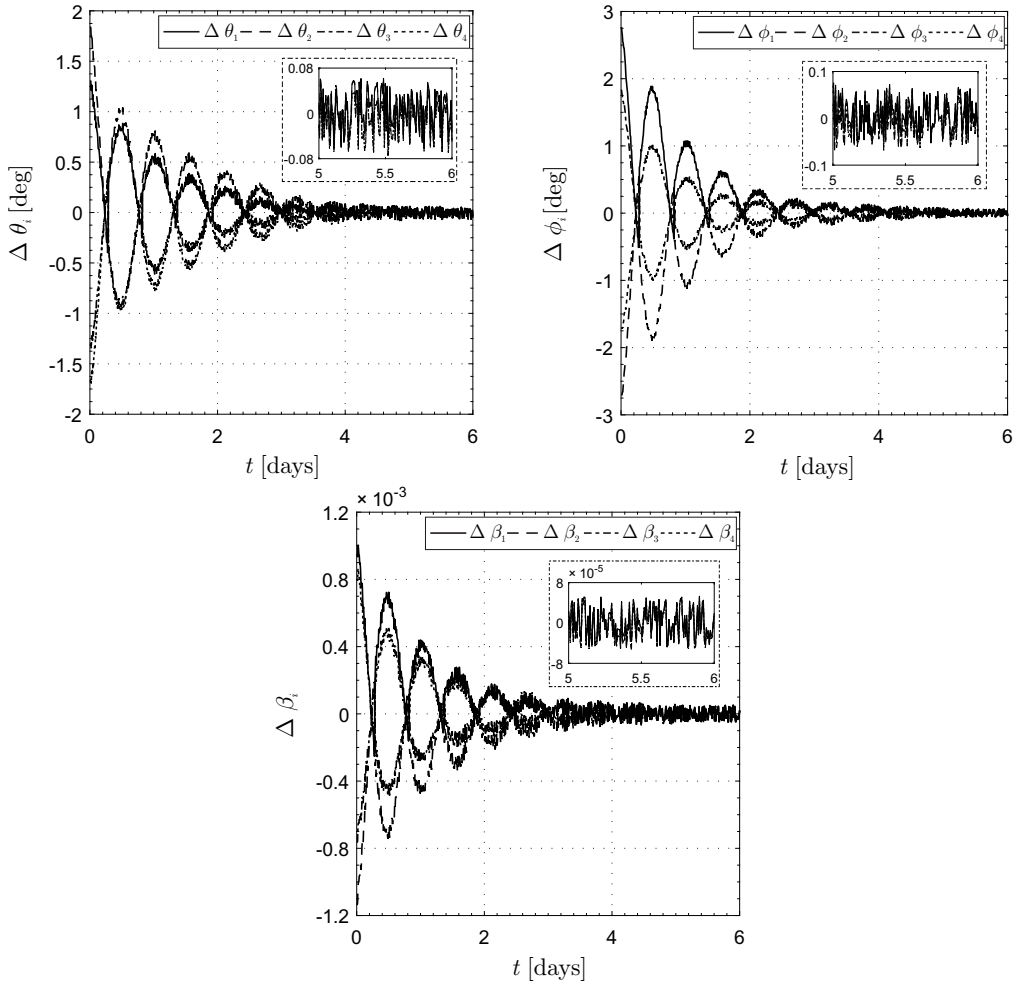

Figure 8: Control input $\boldsymbol{u}_i$ with actuator fault.

6. Acknowledgements

This work was supported by the National Science Fundation of China (Grant nos. 11525208 and 11902175), Postdoctoral Science Foundation of China (Grant nos. BX20190166 and 2019M650700), and University of Pisa, Progetti di Ricerca di Ateneo (Grant no. PRA_2018_44).

References

[1] P. Janhunen, Electric sail for spacecraft propulsion, Journal of Propulsion and Power 20 (4) (2004) 763–764, doi: 10.2514/1.8580.

[2] A. A. Quarta, G. Mengali, Minimum-time trajectories of electric sail with advanced thrust model, Aerospace Science and Technology 55 (2016) 419–430, doi: 10.1016/j.ast.2016.06.020.

[3] M. Huo, G. Mengali, A. A. Quarta, N. Qi, Electric sail trajectory design with Bezier curve-based shaping approach, Aerospace Science and Technology 88 (2019) 126–135, doi: 10.1016/j.ast.2019.03.023.

[4] W. Wang, G. Mengali, A. A. Quarta, J. Yuan, Analysis of relative motion in non-Keplerian orbits via modified equinoctial elements, Aerospace Science and Technology 58 (8) (2016) 389–400, doi: 10.1016/j.ast.2016.09.001.

[5] P. Janhunen, P. K. Toivanen, J. Polkko, et al., Electric solar wind sail toward test missions, Review of Scientific Instruments 81 (11) (2010) 111301–1–111301–11, doi: 10.1063/1.3514548.

[6] L. Niccolai, A. A. Quarta, G. Mengali, Electric sail-based displaced orbits with a refined thrust model, Proceedings of the Institution of Mechanical Engineers, Part G: Journal of Aerospace Engineering 232 (3) (2018) 423–432, doi: 10.1177/0954410016679195.

[7] G. Aliasi, G. Mengali, A. A. Quarta, Artificial equilibrium points for electric sail with constant attitude, Journal of Spacecraft and Rockets 50 (6) (2013) 1295–1298, doi: 10.2514/1.A32540.

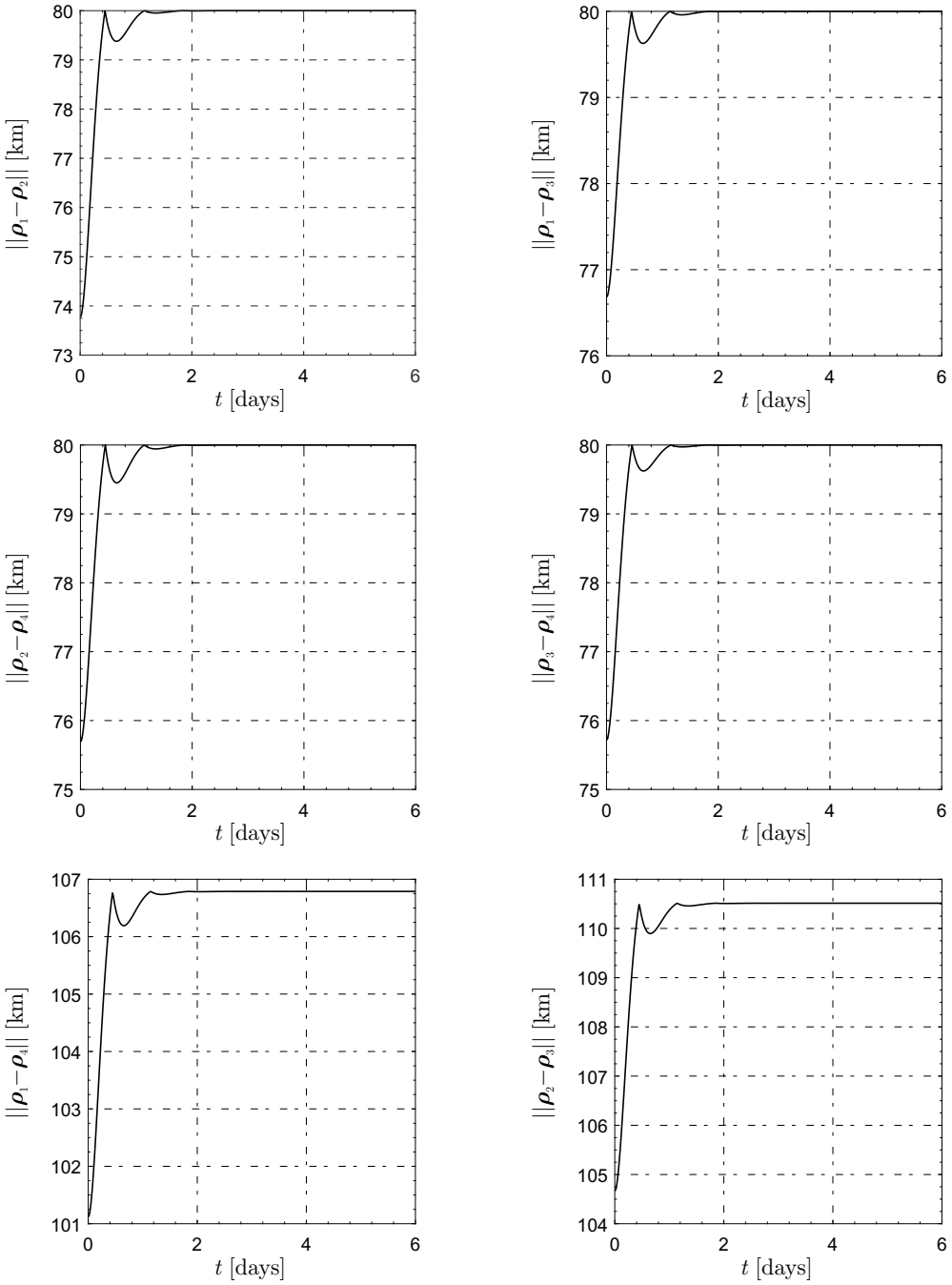

Figure 9: Relative distances without actuator fault.

[8] M. Xu, Y. Liang, X. Fu, Formation flying on quasi-halo orbits in restricted Sun-Earth/Moon system, Aerospace Science and Technology 67 (2017) 118–125, doi: 10.1016/j.ast.2017.03.038.

[9] W. Wang, G. Mengali, A. A. Quarta, J. Yuan, Distributed adaptive synchronization for multiple spacecraft formation flying around Lagrange point orbits, Aerospace Science and Technology 74 (2018) 93–103, doi: 10.1016/j.ast.2018.01.007.

[10] W. Wang, G. Mengali, A. A. Quarta, J. Yuan, Formation flying for electric sails in displaced orbits. part i: Geometrical analysis, Advances in Space Research 60 (6) (2017) 1115–1129, doi: 10.1016/j.asr.2017.05.015.

[11] W. Wang, G. Mengali, A. A. Quarta, J. Yuan, Formation flying for electric sails in displaced orbits. part ii: Distributed coordinated control, Advances in Space Research 60 (6) (2017) 1130–1147, doi: 10.1016/j.asr.2017.06.017.

[12] X. Pan, A. A. Quarta, G. Mengali, M. Xu, Linearized relative motion and proximity control of E-sail-based displaced orbits, (in press). Aerospace Science and Technology, doi: 10.1016/j.ast.2019.105574.

[13] P. K. Toivanen, P. Janhunen, Spin plane control and thrust vectoring of electric solar wind sail, Journal of Propulsion and

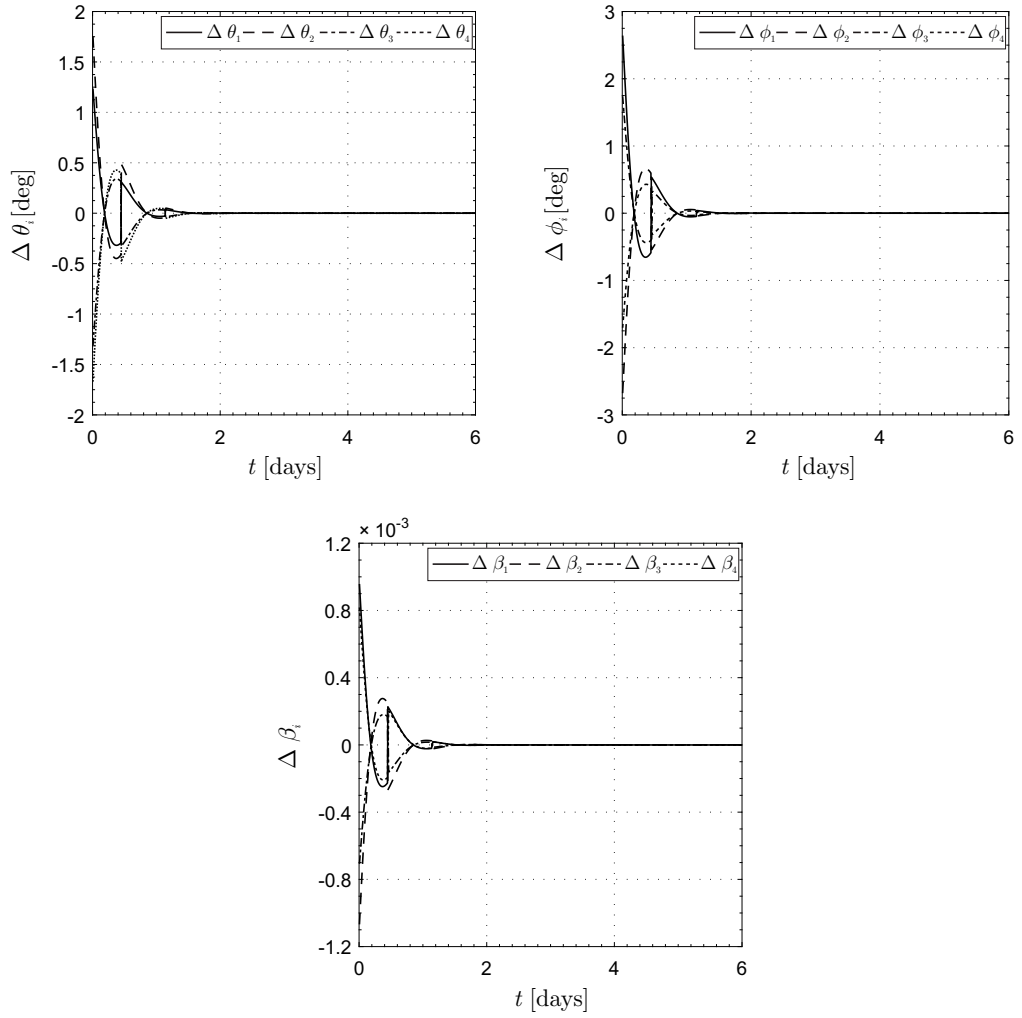

Figure 10: Control input $\boldsymbol{u}_i$ without actuator fault.

Power 29 (1) (2013) 178–185, doi: 10.2514/1.B34330.

[14] P. Janhunen, A. A. Quarta, G. Mengali, Electric solar wind sail mass budget model, Geoscientific Instrumentation, Methods and Data Systems 2 (1) (2013) 85–95, doi: 10.5194/gi-2-85-2013.

[15] F. Liu, Q. Hu, Y. Liu, Attitude dynamics of electric sail from multibody perspective, Journal of Guidance, Control, and Dynamics 41 (12) (2018) 2633–2646, doi: 10.2514/1.G003625.

[16] Y. Wang, B. Bian, Trajectory tracking control of electric sail with input uncertainty and saturation constraint, Transactions of the Institute of Measurement and Control 39 (7) (2017) 1007–1016, doi: 10.1177/0142331215625771.

[17] L. Niccolai, A. Anderlini, G. Mengali, A. A. Quarta, Impact of solar wind fluctuations on electric sail mission design, Aerospace Science and Technology 82–83 (2018) 38–45, doi: 10.1016/j.ast.2018.08.032.

[18] C. R. McInnes, A. J. C. McDonald, J. F. L. Simmons, E. W. MacDonald, Solar sail parking in restricted three-body systems, Journal of Guidance, Control, and Dynamics 17 (2) (1994) 399–406, doi: 10.2514/3.21211.

[19] M. Huo, G. Mengali, A. A. Quarta, Electric sail thrust model from a geometrical perspective, Journal of Guidance, Control and Dynamics 41 (3) (2018) 735–741, doi: 10.2514/1.G003169.

[20] M. Bassetto, G. Mengali, A. A. Quarta, Stability and control of spinning E-sail in heliostationary orbit, Journal of Guidance, Control, and Dynamics 42 (2) (2019) 425–431, doi: 10.2514/1.G003788.

[21] W. Ren, R. W. Beard, E. M. Atkins, Information consensus in multivehicle cooperative control, IEEE Control Systems Magazine 27 (2) (2007) 71–82, doi: 10.1109/MCS.2007.338264.

[22] W. Wang, G. Mengali, A. A. Quarta, J. Yuan, Multiple solar sail formation flying around heliocentric displaced orbit via consensus, Acta Astronautica 154 (2019) 256–267, doi: 10.1016/j.actaastro.2018.03.039.

[23] Y. Cao, W. Ren, Distributed coordinated tracking with reduced interaction via a variable structure approach, IEEE Transactions on Automatic Control 57 (1) (2012) 33–48, doi: 10.1109/TAC.2011.2146830.

[24] H. G. Tanner, A. Jadbabaie, G. J. Pappas, Flocking in fixed and switching networks, IEEE Transactions on Automatic Control 52 (5) (2007) 178–185, doi: 10.1109/TAC.2007.895948.

[25] Y. Wang, Y. Song, F. L. Lewis, Robust adaptive fault-tolerant control of multiagent systems with uncertain nonidenti-

cal dynamics and undetectable actuation failures, Transactions on Industrial Electronics 62 (6) (2015) 3978–3988, doi: 10.1109/TIE.2015.2399400.
[26] G. Chen, Y. Song, Robust fault-tolerant cooperative control of multi-agent systems: A constructive design method, Journal of the Franklin Institute 352 (10) (2015) 4045–4066, doi: 10.1016/j.jfranklin.2015.05.031.
[27] J. E. Slotine, W. Li, Applied Nonlinear Control, NJ: Prentice-Hall, New York, 1991, pp. 124–128.
[28] D. Izzo, L. Pettazzi, Autonomous and distributed motion planning for satellite swarm, Journal of Guidance, Control, and Dynamics 30 (2) (2007) 449–459, doi: 10.2514/1.22736.